

Article

Effects of Homogenization Conditions on the Microstructure Evolution of Aluminium Alloy EN AW 8006

Maja Vončina ^{1,*} , Kristijan Kresnik ¹, Darja Volšak ² and Jožef Medved ¹

¹ University of Ljubljana, Faculty of Natural Sciences and Engineering, Department for Materials and Metallurgy, Aškerčeva 12, Ljubljana, Slovenia; kristijankresnik@gmail.com (K.K.); jozef.medved@omm.ntf.uni-lj.si (J.M.)

² Impol Aluminium Industry d.d., Partizanska 38, 2310 Slovenska Bistrica, Slovenia; darja.volsak@impol.si

* Correspondence: maja.voncina@omm.ntf.uni-lj.si; Tel.: +00386-1-2000418

Received: 28 February 2020; Accepted: 22 March 2020; Published: 24 March 2020



Abstract: The industrial production of products, such as foil and aluminium alloy strips, begins with the production of semi-finished products in the form of slabs. These are produced by the continuous casting process, which is quick and does not allow the equilibrium conditions of solidification. Non-homogeneity—such as micro and macro segregation, non-equilibrium phases and microstructural constituents, as well as stresses arising during non-equilibrium solidification—are eliminated by means of homogenization annealing. In this way, a number of technological difficulties in the further processing of semi-finished products can be avoided. The aim of this research was the optimization of the homogenization annealing of the EN AW 8006 alloy. With the Thermo-Calc software, a thermodynamic simulation of equilibrium and non-equilibrium solidification was performed. Differential scanning calorimetry (DSC) was performed on selected samples in as-cast state and after various regimes of homogenization annealing and was used for the simulation of homogenization annealing. Using an optical microscope (OM), a scanning electron microscope (SEM) and an energy dispersion spectrometer (EDS), the microstructure of the samples was examined. Based on the results, it was concluded that homogenization annealing has already taken place after 8 h at 580 °C to the extent, that the material is then suitable for further processing.

Keywords: wrought aluminium alloy; homogenization annealing; thermodynamic equilibrium; microstructure; intermetallic phases; differential scanning calorimetry (DSC)

1. Introduction

Due to their relatively high strength, combined with their sufficient ductility, the non-hardenable alloys Al-Fe-Mn-Si are largely used in the automotive industry, cooling systems, civil engineering, etc. Al-foil can be produced either by starting from a conventional direct chill (DC) cast ingot which is then hot rolled to a strip of about 2–5 mm, or from continuous casting a 6–7-mm-thick sheet (twin roll casting or belt casting) and then cold rolling it to an intermediate (foil stock) gauge of about 0.4–1 mm. This is followed by annealing in the temperature range 350–400 °C. [1] Then, the material is cold rolled to final foil thickness. Afterwards, closed gap rolling must be used to achieve thinner foil gauges below 100 µm, which is performed in a dedicated foil mill. Most Al-foil products will be used in the O-temper conditions (foil must be soft annealed). In addition to the recrystallization, the final gauge annealing is required to remove lubricant from the foil [2].

Thin aluminium sheets which exhibit good formability and sufficient rigidity are advisable for use in applications such as fin-stocks in heat exchangers. Thus, a fine grain size structure and a texture warranting low anisotropy must be achieved by alloy processing. The form in which alloying

elements are present is an important factor influencing recrystallization and texture development, and in consequence alloy properties. Iron, manganese and silicon may be present in second-phase particles or dissolved in the matrix. Coarse intermetallic particles usually act as nucleation sites during recrystallization, giving a random or retained rolling texture. Fine particles inhibit grain growth by pinning grain boundaries. Thus, depending on dispersoid density and size, recrystallization can be accelerated or retarded. Alloying elements in a solid solution also affects structure and properties. Solid solution element content and dispersoid distribution can be changed by heat treatment [3–5].

Detailed knowledge of the correlation of the microstructure and processing parameters is required for proper control of the final material's properties. [6,7]. In relatively clean Al-foil alloys, especially the material's microchemistry, i.e., the solution/precipitation state of the alloying elements Fe and Si, and other impurities, will affect both processing and foil properties at the final gauge. Commercial Al-alloys will always comprise large Fe-bearing phases because of the very low solubility of Fe in Al. The type, volume, size, and especially the morphology of these constituent particles have an impact on ductility and formability. Pre-heating or homogenization annealing prior to hot rolling will affect both processing and final foil properties by leading to the formation of fine secondary intermetallic phases or so-called 'dispersoids' [6,7]. The solute level upon hot deformation must be kept low, whereas there is a limitation to the amount of strengthening through solid solution hardening, such that the dominant strengthening mechanism in dilute Al-foil alloys is dispersion hardening, with some contribution from solutes. Hence, the volume fraction and size distribution of the dispersoids is an important factor in dispersion strengthening [8,9]. Increased hardness leads to reduced formability and fatigue resistance as a result of needle-shaped particles. Grain size has a relatively small influence on strength, but largely impacts ductility, with finer grain size giving higher ductility [6,10].

Figure 1a shows the Al-rich corner of the equilibrium ternary phase diagram Al-Fe-Si as a function of the Si and Fe content for the investigated alloy EN AW 8011. [11,12] The diagram displays a total of three different second-phase particles in equilibrium with the Al-matrix (α -Al), for which the stability ranges depend on temperature and the exact Si content. The maximum solubility of Fe in Al is 0.05 wt. % at 650 °C. Accordingly, alloys based on commercial purity will always comprise Fe-bearing constituent phases. Alloys with low Si content usually contain rather large fractions of the phase Al_3Fe (or $\text{Al}_{13}\text{Fe}_4$). This phase adversely affects the formability of Al-foil alloys by forming needle-like particles [13]. Al-alloys with increased Si content over 0.5 wt. % display significant portions of ternary AlFeSi-phases [12]. At medium Si contents and/or high temperatures, the α -AlFeSi phase is obtained, whereas the chemical composition of this phase shows rather large scatter and is described as $\text{Al}_8\text{Fe}_2\text{Si}$ or $\text{Al}_{12}\text{Fe}_3\text{Si}$. The ratio of Fe:Si may vary between 2:1 and 3:1 in at. % or, between 4:1 and 6:1 in wt. %. Increased Si contents and lower temperatures tend to stabilize the phase β -AlFeSi. For this phase a stoichiometric composition of Al_5FeSi is reported; thus, the Fe:Si ratio in at. % is 1:1, and in wt. % this ratio is very close to 2:1 [1].

Analysis of EN AW 8006 alloys at a low content of Si impurity can be considered using an Al-Fe-Mn phase diagram (Figure 1b). The isothermal sections of this diagram in the solid state have only one three phase region (Al) + $\text{Al}_6(\text{FeMn})$ + Al_3Fe . Polythermal sections within the compositional range of EN AW 8006 commercial alloys have only one invariant horizontal. The sections at 0.7 wt. % Mn and 1.6 wt. % Fe show that primary crystals of the Al_3Fe and $\text{Al}_6(\text{FeMn})$ phases can form when the Fe concentration is at the upper limit [14].

Due to dispersion hardening and grain boundary hardening, strain hardening capacity increases simultaneously with an increasing Fe content, which leads to an increase of the tensile strength and a decrease in the grain size, and therefore produces high elongation values. The castability improves from the addition of Si and, furthermore, the cast structure becomes more uniform. Si accelerates the precipitation of dissolved solute elements during annealing. Si contents higher than 0.8 wt. % lower the recrystallization temperature, limit the final anneal temperature range, and reduce the positive effect of Fe on the grain size. Generally, Mn retards recrystallization and increases the recrystallization temperature [15].

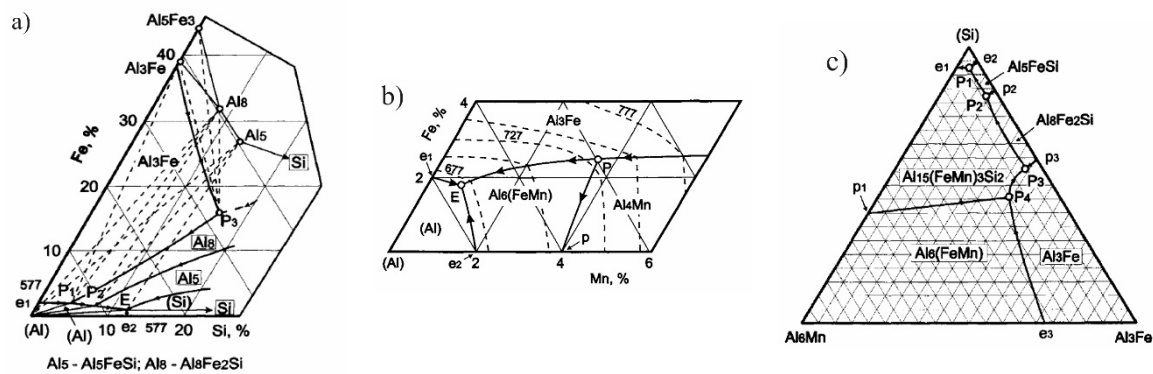


Figure 1. Phase diagram of an Al-Fe-Si system (a), a liquidus projection of an Al-Fe-Mn system (b), and a polythermal projection of the solidification surface of an Al-Fe-Mn-Si system (c) reproduces from reference [12].

The conditions for equilibrium solidification are not fulfilled in practice due to quite high cooling rates prevailing during industrial DC-casting [9]. Therefore, the as-cast ingot will be supersaturated with Fe and by other slow-diffusing species, such as Mn and Cr, if they are present. Under these conditions, a metastable phase Al₆Fe can form in addition to the stable monoclinic Al₃Fe phase. This phase is isomorphous to the orthorhombic Al₆Mn phase usually encountered in Mn-containing alloys (3xxx or 5xxx series alloys) [12]. Furthermore, the literature describes other metastable phases of Al_mFe where m varies from 4 to 5 [14]. A transformation of the metastable Fe-bearing phases towards stable Al₃Fe can be achieved by homogenization at high temperatures [7,16,17]. If Mn is present, the α-AlFeSi phase is replaced by an isostructural quaternary α-Al(Mn,Fe)Si phase from the system presented in Figure 1c, which may show large variation in exact chemical composition [6,16].

The industrial production of products, such as strips and foils, from aluminium alloys starts with a semi-finished product in the form of a slab, which does not allow solidification at equilibrium conditions. Inhomogeneities, micro-segregations, residual stresses and other defects that occur in the material during un-equilibrium solidification are eliminated with homogenization annealing. [1] The more present internal defects are the large AlFeMn and/or AlFeMnSi intermetallic particles with different sizes, which are aligned on the deformation direction. Some zones have a coarse and fragile compound. The agglomeration of intermetallic particles leads to the rupture of the foil. Heat treatment (the homogenization of the alloy at 570 °C/180 min.) can prevent the structure defects observed in sheets and foils produced from EN AW 8006 alloy. [18,19] Aluminium oxide and/or spinel (MgO·Al₂O₃) on the surface of the sheets can be observed. It is more likely for these inclusions to become sources of pinholes in the sheets. Moreover, spherical particles of aluminium boride can be seen on the surface of the sheets. They are small in size and non-deformable particles compared to the ductile aluminium matrix, but they can affect the performance of the sheet rolling [19,20].

Homogenization processing has a critical contribution by allowing the precipitation of excessive alloying elements in the solid solution before subsequent thermomechanical processing. However, the high solidification rate encountered in TRC (twin-roll casting) not only favours the supersaturation and metastable condition of the alloying elements, but also hinders their micro-segregation [21,22].

In the present study, the microstructural evolution of the typical dilute Al-Fe-Si (EN AW 8006) foil alloy during homogenization was investigated using optical and electron microscopy as well as differential scanning calorimetry (DSC). The effect of different homogenization practices on the formation of intermetallic phases was analysed. Especially, the impact of homogenization on changes in the morphology of plate-like constituent particles which are known [23] to adversely affect the formability of 8xxx series alloys was examined.

2. Materials and Methods

The aim of the study was to optimize the homogenization annealing of the EN AW 8006 alloy slab. Standard composition is listed in Table 1.

Table 1. The standard chemical composition of the EN AW 8006 alloy/wt. %.

Element	Si	Fe	Cu	Mn	Mg	Zn	Other	Al
Amount	0.40	1.2–2.0	0.3	0.30–1.0	0.10	0.10	0.05	Bal.

A thermodynamic analysis was conducted using Thermo-Calc Software (TCW2019, Stockholm, Sweden) and TCAL6 database to obtain the phase diagram and the stability of different phases, as well as the equilibrium concentrations of these phases.

Samples for heat treatment investigations were cut from the middle of the front surface of a slab with dimensions of 510 × 1310 × 4800 mm, in the form of cubes. The samples' dimensions were approximately 15 mm (l) × 15 mm (w) × 15 mm (h). Single-step solution heat treatments (homogenization treatments) were done using an electric chamber furnace, which was previously calibrated. For the investigation of solution heat treatments, samples were held for various times—4 h, 6 h, 8 h, 10 h and 12 h—at temperatures of 580 °C and 600 °C to investigate the effect of homogenization on the dissolution of particles. Samples were, after a certain time, removed from the furnace and cooled in air in order to simulate industrial conditions. All metallographic examinations were carried out on half of the samples after homogenization annealing, whereas the remainder were grinded and polished according to the standard metallographic procedure for aluminium alloys. Differential scanning calorimetry (DSC) was performed on samples in an as-cast state and on the second half of the homogenized samples, after different regimes of homogenization annealing, using an STA Jupiter 449c apparatus (NETZSCH Group, Selb, Germany). DSC analysis was performed as follows: heating up to 710 °C, followed by cooling to room temperature using 10 K/min heating and cooling rate in a protective atmosphere of argon. Using an optic microscope Zeiss Axio Observer 7 (ZEISS International, Jena, Germany) and a scanning electron microscope SEM—Jeol JSM 6610LV (JEOL Ltd., Tokyo, Japan) with an energy dispersion spectrometer (EDS), the microstructural components were analysed.

Samples for homogenisation simulation on the DSC apparatus were taken from the middle of the slab. On the DSC device, the homogenization of the as-cast samples was carried out, which lasted for 12 h at 580 °C and 600 °C. By using the tangent method, the change in the slope of the DSC curves was determined, which is also attributed to changes in the course of homogenization.

3. Results and discussion

Figure 2 illustrates the results of the thermodynamic calculations. The results indicate that the temperature range for the dissolution is 550–620 °C. As shown in Figure 2, the equilibrium phases and the temperature ranges in which they are present are: the $Al_{13}Fe_4$ phase up to 652 °C, the $Al_{15}Si_2Mn_4$ phase up to 630 °C, the $Al_9Fe_2Si_2$ phase up to 477 °C, and the Al_6Mn phase up to 444 °C. This implies that by heating at 580 °C or 600 °C for a long holding time, $Al_{15}Si_2Mn_4$ will partially dissolve, and $Al_9Fe_2Si_2$ and Al_6Mn will completely dissolve, but the iron phase $Al_{13}Fe_4$, as well as a fraction of the $Al_{15}Si_2Mn_4$ phase, will still be present. It should also be noted that the homogenization treatment for these alloys should not be conducted at temperatures over 640 °C, as the Fe-rich eutectic phase $Al_{13}Fe_4$ will start to melt.

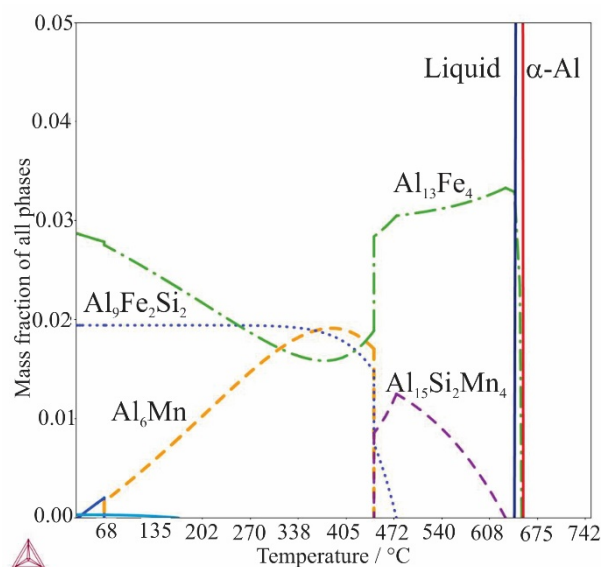


Figure 2. Thermo-Calc predicted phase stability in aluminium alloy EN AW 8006 with regard to the temperature.

In Figure 3, the heating and cooling DSC curves of the experimental samples are presented, whereas only samples in an as-cast state, and after 6 h and 12 h at temperatures of 580 °C and 600 °C, were analysed.

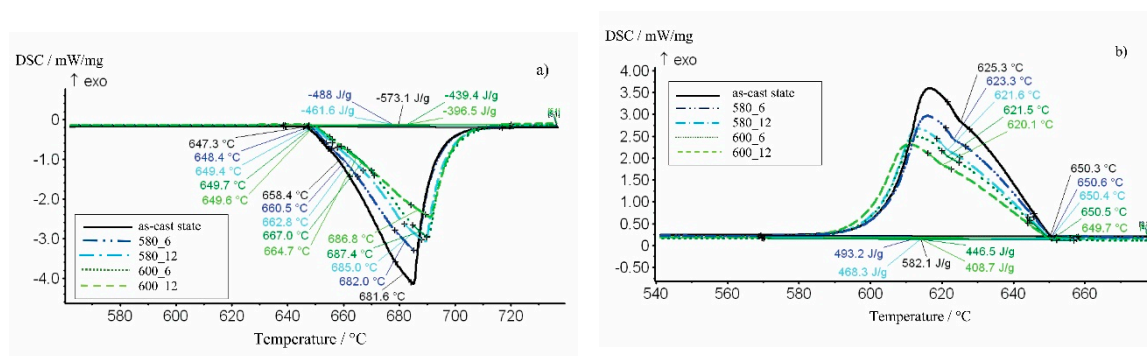


Figure 3. Heating (a) and cooling (b) Differential scanning calorimetry (DSC) curves of the investigated samples after homogenization.

From these results, characteristic temperatures at heating and cooling, as well as melting (ΔH_m) and solidification (ΔH_s) enthalpies were determined.

From Figure 3a it can be determined, according to Thermo-Calc calculations, that at a temperature of about 649 °C the melting of the eutectic with the Mn-phase occurs, at a temperature of about 664 °C the melting of eutectic (α -Al + $\text{Al}_{13}\text{Fe}_4$) occurs, and at a temperature of 685 °C the melting of the primary crystals α -Al takes place. From the cooling DSC curves, the solidification is as follows (Figure 3b): the primary solidification of α -Al occurs at about 650 °C, and the solidification of the eutectic (α -Al + $\text{Al}_{13}\text{Fe}_4$) occurs at a temperature of about 621 °C. The solidification of Mn-phase could not be detected due to an equilibrium solidification.

In order to improve transparency, the temperatures and enthalpies are collected in Table 2. It can be considered that the melting temperature of the Mn-eutectic is the lowest in the sample in the as-cast state (647.3 °C), the melting temperature is increased in homogenized samples, and is the highest (649.7 °C) in samples that were homogenized at 600 °C. This trend is also observed in the second eutectic (α -Al + $\text{Al}_{13}\text{Fe}_4$). The melting temperature of the α -Al phase is also the lowest in the

as-cast state (681.6 °C), which results from a slower and more equilibrus solidification. It is raised by a higher homogenization temperature and a longer homogenization annealing time. It is also observed that the largest melting enthalpy is in the sample in the as-cast state (−573.1 J/g). Homogenized samples have a lower melting enthalpy, where the lowest is in the sample after homogenization at 600 °C 12 h.

Table 2. Listed melting and solidification temperatures, as well as corresponding enthalpies.

Sample	Heating/Melting			Cooling/Solidification			
	ΔH_m (J/g)	$T_{Al_{15}Si_2Mn_4}$ (°C)	$T_{Al_{13}Fe_4}$ (°C)	$T_{\alpha-Al}$ (°C)	ΔH_s (J/g)	$T_{\alpha-Al}$ (°C)	$T_{Al_{13}Fe_4}$ (°C)
As cast	−73.1	647.3	658.4	681.6	582.1	650.3	625.3
580-6	−488	648.4	660.5	682.0	493.2	650.6	623.3
580-12	−461.6	649.4	662.8	685.0	486.3	650.4	621.6
600-6	−439.4	649.7	667.0	687.4	446.5	650.5	621.5
600-12	−396.5	649.6	664.7	686.8	408.7	649.7	620.1

The liquidus temperatures of all samples are around 650 °C. At cooling, only the primary solidification and the solidification of the eutectic (α -Al + $Al_{13}Fe_4$) can be observed on the cooling DSC curve, which results from a slower and more equilibrus solidification. The liquidus temperature does not change significantly with the time and temperature of the prior homogenization annealing. The highest solidification temperature of the eutectic (α -Al + $Al_{13}Fe_4$) is in the sample in the cast state (625.3 °C), which decreases with increasing homogenization temperature and time. The tendency of the solidification enthalpy variation is the same as in the melting enthalpy.

These observations correlate with the fact that the effects of homogenization are greater for longer periods and higher annealing temperatures.

The optical micrographs taken from samples after various homogenization regimes are shown in Figures 4 and 5. In the as-cast sample, there is at most a finely dispersed eutectic that occurs during longer $Al_{13}Fe_4$ needles. A slightly larger square phase of $Al_{15}Si_2Mn_4$ irregular forms is also observed. In homogenized samples, dispersed phases, which look like $Al_{13}Fe_4$, appear in the α -Al matrix. The eutectic phase $Al_{15}Si_2Mn_4$ gradually dissolves and disappears with longer annealing times. Those which remain become slightly larger and rounded, which is desirable due to their lower cut effect and thus their better forming properties. The longer needle phases $Al_{13}Fe_4$ become more rounded by increasing the annealing time. Similarly, it occurs at both temperatures, but at a higher temperature of annealing (Figure 5) the less eutectic phase is seen, which is somewhat more rounded. The content and shape of the intermetallic phases does not change significantly after eight hours of annealing.

In addition, the simulation of the homogenization was done using DSC measurement, whereas the homogenization process was analysed at two experimental temperatures, 590 °C and 610 °C, respectively. Each experiment was performed two times; the results are presented in Figure 6. The results show that when homogenization takes place at 590 °C, not all phases are dissolved in 12 h, but rather that the process is continuing, whereas the DSC curve is still dropping. At 610 °C, most of the homogenization process is finished after 160 min, and fully finished after 300 min, at 610 °C. These results are in good agreement with the microstructure results in Figures 4 and 5.

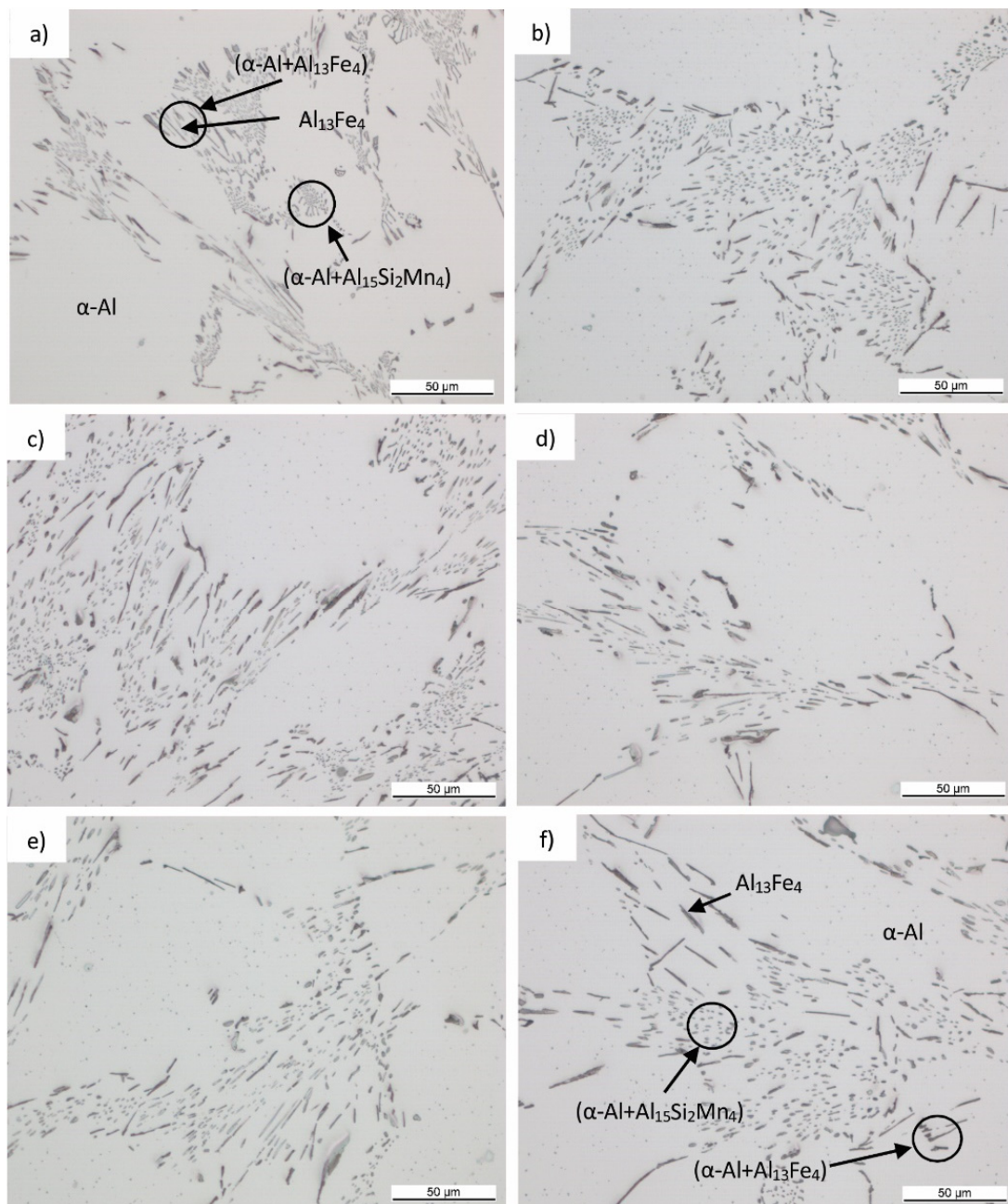


Figure 4. Microstructure of a sample in an as-cast state, and of homogenized samples at 580 °C, at 500× magnification: in an as-cast state (a) and after 4 h (b), 6 h (c), 8 h (d), 10 h (e) and 12 h (f).

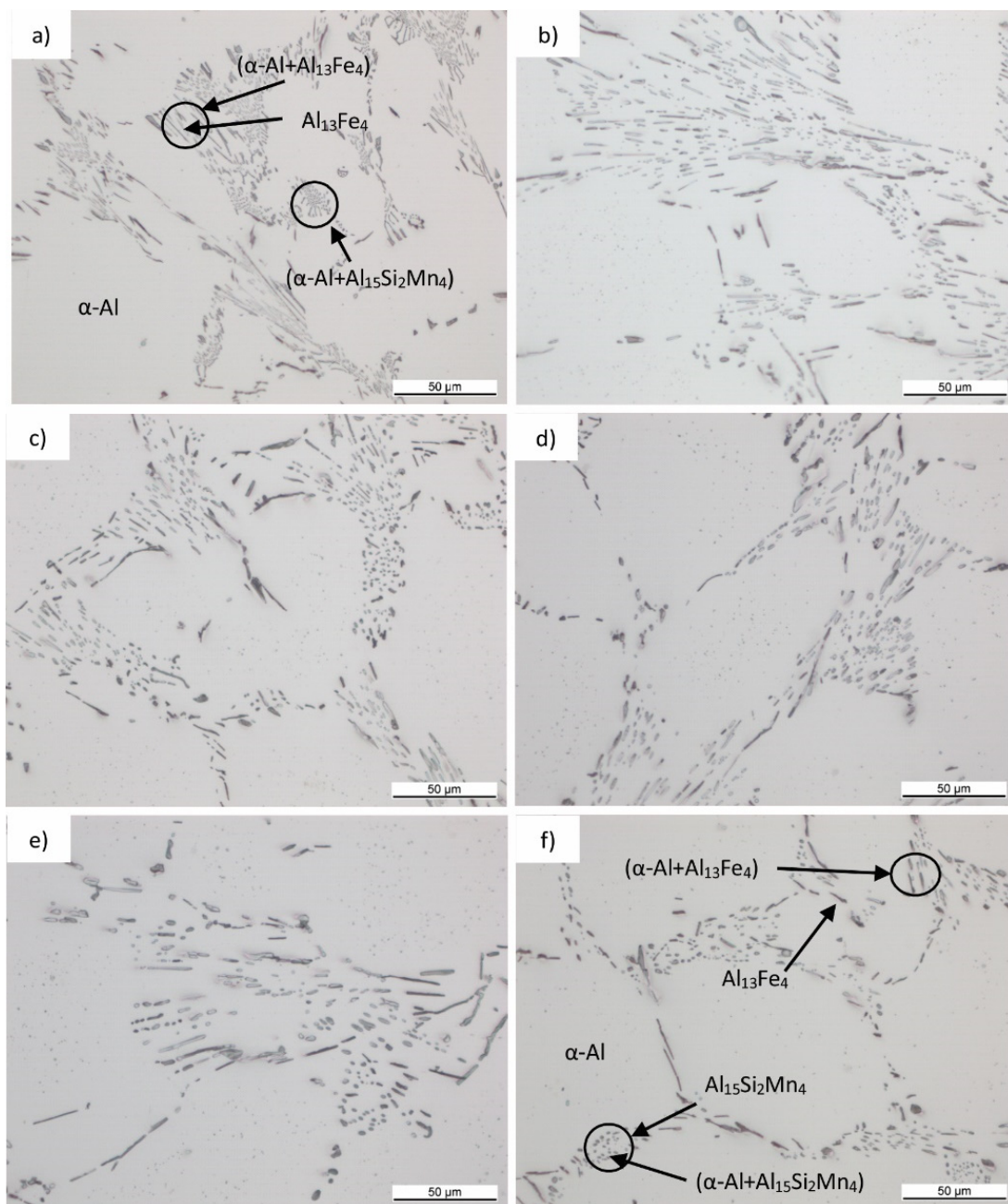


Figure 5. Microstructure of sample in as-cast state and homogenized samples at 600 °C at 500× magnification: in as-cast state (a) and after 4 h (b), 6 h (c), 8 h (d), 10 h (e) and 12 h (f).

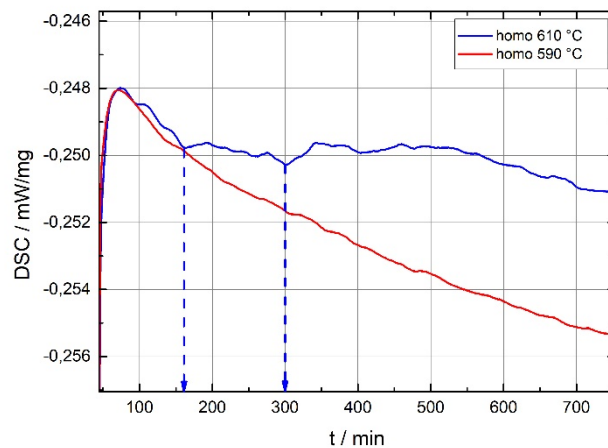


Figure 6. DSC measurement of homogenization annealing of EN AW 8006 alloy at 590 °C and 610 °C.

Furthermore, an EDS analysis of the selected samples (Figure 7) was made in order to determine the type and phase composition of phases after certain homogenization regimes. From the EDS analysis, listed in Table 3, it can be concluded that the phases in the form of large, sharp needles contain mainly aluminium and iron, which indicates that this is the $\text{Al}_{13}\text{Fe}_4$ phase. Phases of smaller and rounded forms contain a slightly higher concentration of manganese and silicon, indicating that this is the $\text{Al}_{15}\text{Si}_2\text{Mn}_4$ phase. The proportion of these two elements increases in these phases with a longer period of homogenization annealing and is in the as-cast sample up to 2 wt. %, and in the sample 580–12 as well as up to 4 mas. %.

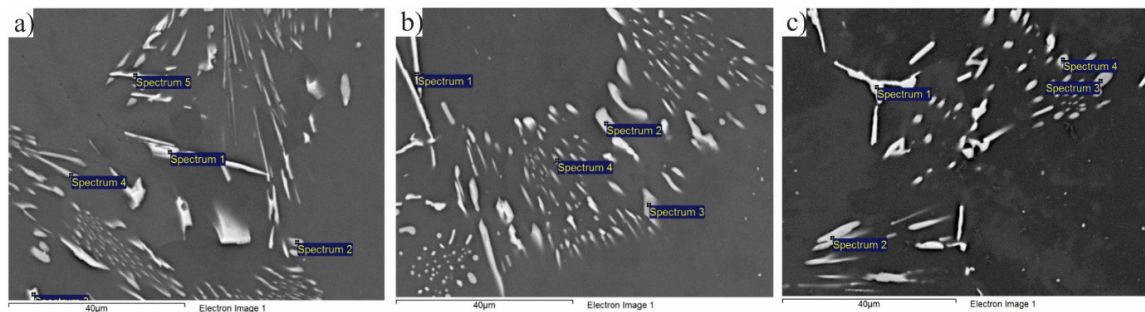


Figure 7. SEM (scanning electron microscope) micrographs of the as-cast sample (a), and the samples homogenized for 6 h (b) and 12 h (c) at a temperature of 580 °C, wherein EDS (energy dispersion spectrometer) analysed spots are marked.

Table 3. EDS results showing different phases present in the investigated samples from Figure 7 in at. %.

State	As-Cast					580-6				580-12			
Element	1	2	3	4	5	1	2	3	4	1	2	3	4
Al	77.96	87.36	78.47	91.1	83.03	82.05	78.92	88.58	91.08	79.01	79.68	85.65	82.76
Si	1.43	0.34	1.39	0.22	1.03	0.71	3.93	2.91	0.15	0.81	4.43	1.2	4.15
Mn	1.14	1.5	1.27	1.1	0.82	0.86	2.42	2.16	1.75	1.13	3.07	2.47	2.84
Fe	19.46	10.8	18.87	7.59	15.11	16.38	14.74	6.35	7.02	19.05	12.82	10.69	10.25
Estimated phase	Al ₁₅ Si ₂ Mn ₄	-	Al ₁₅ Si ₂ Mn ₄	Al ₁₃ Fe ₄	Al ₁₃ Fe ₄	Al ₁₃ Fe ₄	Al ₁₅ Si ₂ Mn ₄	Al ₁₅ Si ₂ Mn ₄	-	Al ₁₃ Fe ₄	Al ₁₅ Si ₂ Mn ₄	Al ₁₅ Si ₂ Mn ₄	Al ₁₅ Si ₂ Mn ₄

Table 4. EDS results showing different phases present in the investigated samples from Figure 8 in at. %.

State	600-4					600-6					600-12				
Element	1	2	3	4	5	1	2	3	4	5	1	2	3	4	5
Al	79.41	86.63	81.55	80.52	90.11	83.04	80.16	79.45	81.15	91.61	88.2	77.44	84.59	81.39	85.21
Si	0.95	0.07	0.88	0.83	0.14	0.79	0.7	0.78	4.72	0.14	0.72	0.77	4.12	0.76	0.55
Mn	1.73	2.47	1.24	1.25	2.06	1.35	1.05	1.29	3.2	2	1.24	1.32	3.02	1.53	1.21
Fe	17.91	10.83	16.33	17.41	7.69	14.82	18.09	18.48	10.94	6.25	17.83	20.47	8.27	15.78	13.04
Estimated phase	Al ₁₃ Fe ₄	-	Al ₁₃ Fe ₄	Al ₁₃ Fe ₄	-	Al ₁₃ Fe ₄	Al ₁₃ Fe ₄	Al ₁₃ Fe ₄	Al ₁₅ Si ₂ Mn ₄	-	Al ₁₃ Fe ₄	Al ₁₃ Fe ₄	Al ₁₅ Si ₂ Mn ₄	Al ₁₃ Fe ₄	Al ₁₃ Fe ₄

For samples that were homogenized at 600 °C (Figure 8), the effects of homogenization are even clearer. The needles of the eutectic phase $Al_{13}Fe_4$ grow and become even more pronounced. Mn-phases are slightly less noticeable with a longer homogenization time. They form more roundish, their particles are smaller and accumulate in larger aggregates, whereas the concentration of manganese and silicon increases (Table 4).

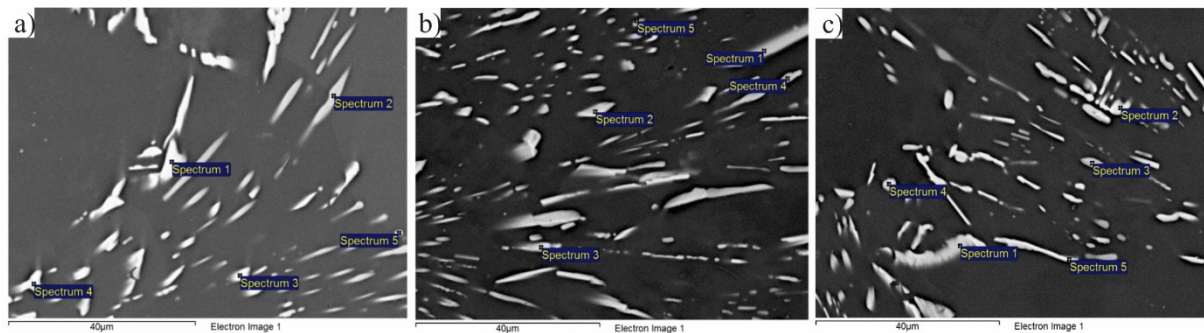


Figure 8. SEM micrographs of samples homogenized for 4 h (a), 6 h (b) and 12 h (c) at a temperature of 600 °C, wherein EDS analysed spots are marked.

4. Conclusions

In this research, the optimization of the homogenization annealing of EN AW 8006 alloy was performed, and the following conclusions were drawn.

In samples of EN AW 8006 alloy, the following phases can occur: α -Al; long needles from the $Al_{13}Fe_4$ phase; finely dispersed (α -Al + $Al_{13}Fe_4$) eutectic; and larger, more square forms of the $Al_{15}Si_2Mn_4$ phase. By prolonging the time of the homogenization annealing, the finely dispersed eutectic (α -Al + $Al_{13}Fe_4$) is partially dissolved in α -Al, and partly forms longer, slightly more rounded needles of the $Al_{13}Fe_4$ phase, which is desirable due to a lower notching effect. The phase $Al_{15}Si_2Mn_4$ also dissolves during homogenization and forms larger globules. It should be noted that the content and shape of the phases after eight hours of annealing does not change significantly at each homogenization temperature.

From the results of EDS phase analysis, it can be concluded that, in the microstructure, there is a solid solution of α -Al and the phase $Al_{13}Fe_4$ and $Al_{15}Si_2Mn_4$, whereas the concentration of silicon and manganese is increased with a longer homogenization time in the $Al_{15}Si_2Mn_4$ phase.

The homogenization annealing time could have been reduced from its current 580 °C for 12 h, wherein preheating takes 5 h, to 6 h at 600 °C, according to DSC and SEM analysis, or to 8 h at 580 °C, according to SEM analysis.

Author Contributions: M.V. carried out the literature review, performed the experiments, analysed the results and wrote the paper. K.K. made the measurements, carried out the metallography and constructed the diagram. D.V. analysed the data and revised the paper. J.M. optimized the research program, improved the idea for the paper, and revised the paper. All authors have read and agreed to the published version of the manuscript.

Funding: This research was supported by Programme P2-0344(B), Functionally graded materials.

Conflicts of Interest: The authors declare no conflict of interest.

References

1. Lentz, M.; Lapyteva, G.; Engler, O. Characterization of second-phase particles in two aluminium foil alloys. *J. Alloy. Compd.* **2016**, *660*, 276–288. [[CrossRef](#)]
2. Kucuk, I. Effect of cold rolling reduction rate on corrosion behaviour of twin-roll cast 8006 Aluminium alloys. *Cumhuriyet Sci. J.* **2018**, *39*, 233–242.
3. Slámová, M.; Očenašek, V.; Dvorak, P.; Juriček, Z. Response of AA 8006 and AA 8111 strip-cast cold rolled alloys to high temperature annealing. *Alum. Alloy.* **1998**, *2*, 1287–1292.

4. Slámová, M.; Očenašek, V.; Dvorak, P.; Juriček, Z. Phase transformation study of two aluminium strip-cast alloys. *Alum. Alloy.* **1998**, *2*, 897–902.
5. Chen, Z.; Zhao, J.; Chen, P. Microstructure and mechanical properties of nanostructured A8006 ribbons. *Mater. Sci. Eng. A* **2012**, *552*, 189–193. [[CrossRef](#)]
6. Engler, O.; Lapyteva, G.; Wang, N. Impact of homogenization on microchemistry and recrystallization of the Al-Fe-Mn Alloy AA 8006. *Mater. Charact.* **2013**, *79*, 60–75. [[CrossRef](#)]
7. Shakiba, M.; Parson, N.; Chen, X.-G. Effect of homogenization treatment and silicon content on the microstructure and hot work ability of dilute Al-Fe-Si alloys. *Mater. Sci. Eng. A* **2014**, *619*, 180–189. [[CrossRef](#)]
8. Roy, R.K.; Kar, S.; Das, S. Evolution of microstructure and mechanical properties during annealing of cold-rolled AA8011 alloy. *J. Alloy. Compd.* **2009**, *468*, 122–129. [[CrossRef](#)]
9. Goulart, P.R.; Lazarine, V.B.; Leal, C.V.; Spinelli, J.E.; Cheung, N.; Garcia, A. Investigation of intermetallics in hypoeutectic Al-Fe alloys by dissolution of the Al matrix. *Intermetallics* **2009**, *17*, 753–761. [[CrossRef](#)]
10. Slámová, M. Effect of strain level on recrystallisation response of AA8006 and AA8011 thin strips. In Proceedings of the METAL 2001, Ostrava, Czech Republic, 15–17 May 2001.
11. Bale, C.W.; Chartrand, P.; Degterov, S.A.; Eriksson, G.; Hack, K.; Mahfoud, B.R.; Melançon, J.; Pelton, A.D.; Petersen, S. Factsage thermochemical software and databases. *Calphad* **2002**, *26*, 189–228. [[CrossRef](#)]
12. Belov, N.A.; Eskin, D.G.; Aksenov, A.A. *Multicomponent Phase diagrams, Applications for Commercial Aluminum Alloys*; Elsevier: Amsterdam, The Netherlands, 2005; p. 424.
13. Wang, X.; Guan, R.G.; Misra, R.D.K.; Wang, Y.; Li, H.C.; Shang, Y.Q. The mechanistic contribution of nanosized Al₃Fe phase on the mechanical properties of Al-Fe alloy. *Mater. Sci. Eng. A* **2018**, *724*, 452–460. [[CrossRef](#)]
14. Belov, N.A.; Aksenov, A.A.; Eskin, D.G. *Iron in Aluminum Alloys: Impurity and Alloying Element*; CRC Press: Boca Raton, FL, USA, 2002; p. 360.
15. Santora, E.; Berneder, J.; Simetsberger, F.; Doberer, M. Mechanical properties evolution for 8xxx foil stock materials by alloy optimization—Literature review and experimental research. In *Light Metals 2019*; Springer: Cham, Switzerland, 2019; pp. 365–372.
16. Li, Y.J.; Arnberg, L. A eutectoid phase transformation for the primary intermetallic particle from Al_m(Fe,Mn) to Al₃(Fe,Mn) in AA5182 alloy. *Acta Mater.* **2004**, *52*, 2945–2952. [[CrossRef](#)]
17. Slámová, M.; Karlík, M.; Cieslar, M.; Chalupa, B.; Merle, P.; Structure transformations during annealing of twin-roll cast Al-Fe-Mn-Si (AA 8006) alloy sheets I. Effect of cold rolling and heating rate. *Kovové Materiály* **2002**, *40*, 389–401.
18. Stanica, C.; Moldovan, P.; Dobra, G.; Bojin, D.; Stanescu, C. Characterization of the microstructure of the AA8006 alloy sheets and foils. In *Light Metals 2008*; TMS (The Minerals, Metals & Materials Society): New Orleans, LA, USA, 2008; pp. 703–707.
19. Băjenaru, O.; Moldovan, P.; Bojin, D. Defects in the AA8006 aluminum alloy sheets. *UPB Sci. Bull. Ser. B Chem. Mater. Sci.* **2008**, *70*, 103–108.
20. Moldovan, P.; Popescu, G.; Miculescu, F. Microscopic study regarding the microstructure evolution of the 8006 alloy in the plastic deformation process. *J. Mater. Process. Technol.* **2004**, *153*, 408–415. [[CrossRef](#)]
21. Chen, Z.; Li, S.; Zhao, J. Homogenization of twin-roll cast A8006 alloy. *Trans. Nonferrous Metal Soc. Chin.* **2012**, *22*, 1280–1285. [[CrossRef](#)]
22. Sadeghi, I.; Wells, M.A.; Esmaeili, S. Modeling homogenization behavior of Al-Si-Cu-Mg aluminum alloy. *Mater. Des.* **2017**, *128*, 241–249. [[CrossRef](#)]
23. Allena, C.M.; O'Reilly, K.A.Q.; Cantor, B.; Evans, P.V. Intermetallic phase selection in 1XXX Al alloys. *Prog. Mater. Sci.* **1998**, *43*, 89–170. [[CrossRef](#)]

